Expanded View Figures

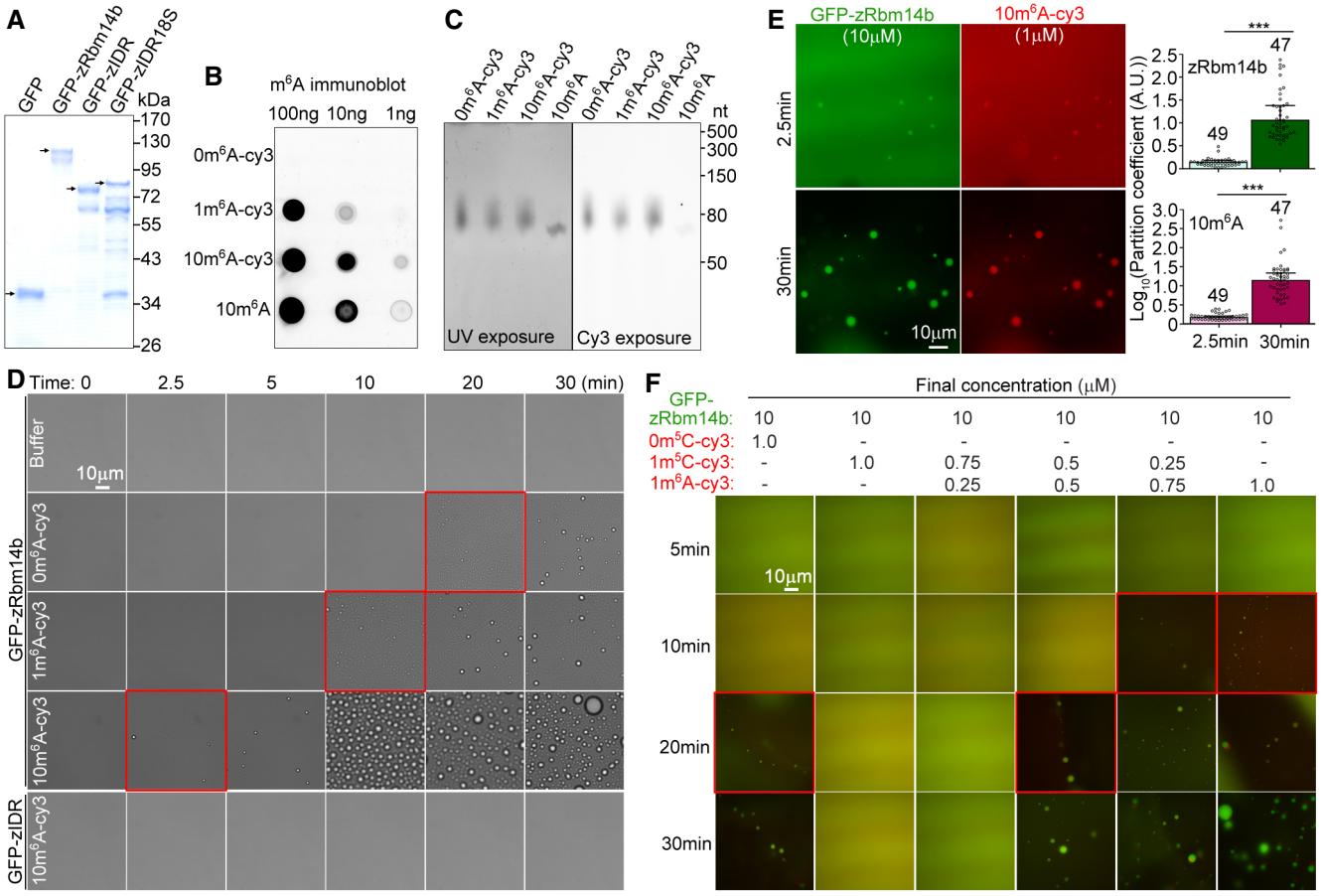

Figure EV1. Proteins and 63-mer RNA fragments used for *in vitro* phase separation assays and time-dependent effect of 10m^{6}A-cy3 on LLPS of zRbm14b (related to Fig 3).

A Purified proteins from *Escherichia coli*. The proteins were subjected to SDS–PAGE and stained with Coomassie Blue. Arrowheads indicate the full-length band of each protein.

B, C Validation of the quality of RNA fragments. *In vitro* transcribed 63-mer RNA fragments were subjected to immuno-northern dot blotting using an anti-m^{6}A antibody (B) or resolved in 15% urea-denaturing PAGE followed by fluorescent imaging to visualize RNA (UV exposure) and the cy3 label (cy3 exposure) (C).

D Representative differential interference contrast images at the indicated time points after the addition of the indicated RNA fragments or buffer into GFP-zRbm14b or GFP-zIDR. The final concentrations of RNAs and proteins were 1 μM and 10 μM, respectively. Imaging was performed at 25°C. Red squares highlight the time of initial LLPS in each group. The results are summarized in Fig 3B.

E Kinetics of 10m^{6}A-induced LLPS of zRbm14b. 10m^{6}A-cy3 was mixed with His-GFP-zRbm14b at the indicated final concentrations and imaged at 25°C. Partition coefficients were respectively calculated for 49 or 47 droplets from three independent experiments and pooled together in the histograms.

F Representative fluorescent images showing effects of m^{6}A- and m^{5}C-RNA modifications on the LLPS of zRbm14b. Imaging was performed at 25°C. Red squares highlight the time of initial LLPS in each group. The results are summarized in Fig 3E.

Data information: Fluorescent micrographs in (E) and (F) were taken manually under a wide-field microscope. Sometimes some condensates moved during imaging, resulting in a positional shift between their GFP and cy3 images. Quantification results are presented as mean ± SD. Unpaired two-sided Student's *t*-test: ***$P < 0.001$. Source data are available online for this figure.

Figure EV2. zRbm14 functions in the blastula-to-gastrula development through both RNA-binding and phase separation (related to Figs 4 and 5A–C).

A Diagrams showing target sequences of the indicated MOs on zRbm14 mRNAs. Translation initiation codons (AUG) are shown in red. Lowercase letters represent intron sequences. 14a-MO and 14b-tMO were designed to respectively repress the translation of both maternal and zygotic mRNAs of zRbm14a and zRbm14b. 14b-MO was designed to interfere with the splicing of zRbm14b pre-mRNA and thus only interfered with the zygotic transcript. The efficacies of both 14a-MO and 14b-MO were confirmed previously using 24-hpf morphants (Xiao *et al*, 2019).

B Our anti-zRbm14a antibody only weakly cross-reacted with zRbm14b. HEK293T cell lysates expressing GFP, GFP-zRbm14a, or GFP-zRbm14b were immunoblotted with antibodies against GFP and zRbm14a, respectively.

C 14a-MO efficiently repressed the translation of zRbm14a mRNA in early embryos. Zebrafish 1-cell embryos were each microinjected with 4 ng of MO and collected at the indicated time points. Lysates from 5 embryos were loaded in each lane. α-tubulin served as an internal control.

D, E 14b-tMO efficiently repressed the translation of zRbm14b mRNA in early embryos. 14b-200 nt-GFP, a reporter mRNA *in vitro* transcribed from a construct containing a 5′ 200-nucleotide zRbm14b cDNA fragment followed by an in-frame GFP cDNA (D), was used to assess the efficacy of 14b-tMO. In total, 100 pg of the reporter mRNA were co-injected with 4 ng of MO into each 1-cell embryo. The embryos were imaged at the indicated time points (E). Note that the embryos co-injected with 14b-tMO failed to express GFP.

F A typical set of zebrafish morphants. In total, 8 ng of ctrl-MO, 14-tMOs (4 ng 14a-MO + 4 ng 14b-tMO), or 14-MOs (4 ng 14a-MO + 4 ng 14b-MO) were co-injected with 100 pg of *in vitro* transcribed GFP mRNA (as a tracer) into each 1-cell embryo to generate control, maternal zRbm14, and zygotic zRbm14 morphants, respectively. GFP-positive embryos were collected at 2.5 hpf and imaged sequentially at the indicated time points. Representative embryos and quantification results are presented in Fig 4A and B.

G A typical set of zebrafish embryos in rescue experiments. 800 pg of *in vitro* transcribed mRNA for one of the indicated proteins were co-injected with 14-tMOs (4 ng 14a-MO + 4 ng 14b-tMO) into 1-cell embryos. GFP-positive morphants were imaged at the indicated time points. Representative embryos (arrows) and quantification results are presented in Fig 5B and C.

Source data are available online for this figure.

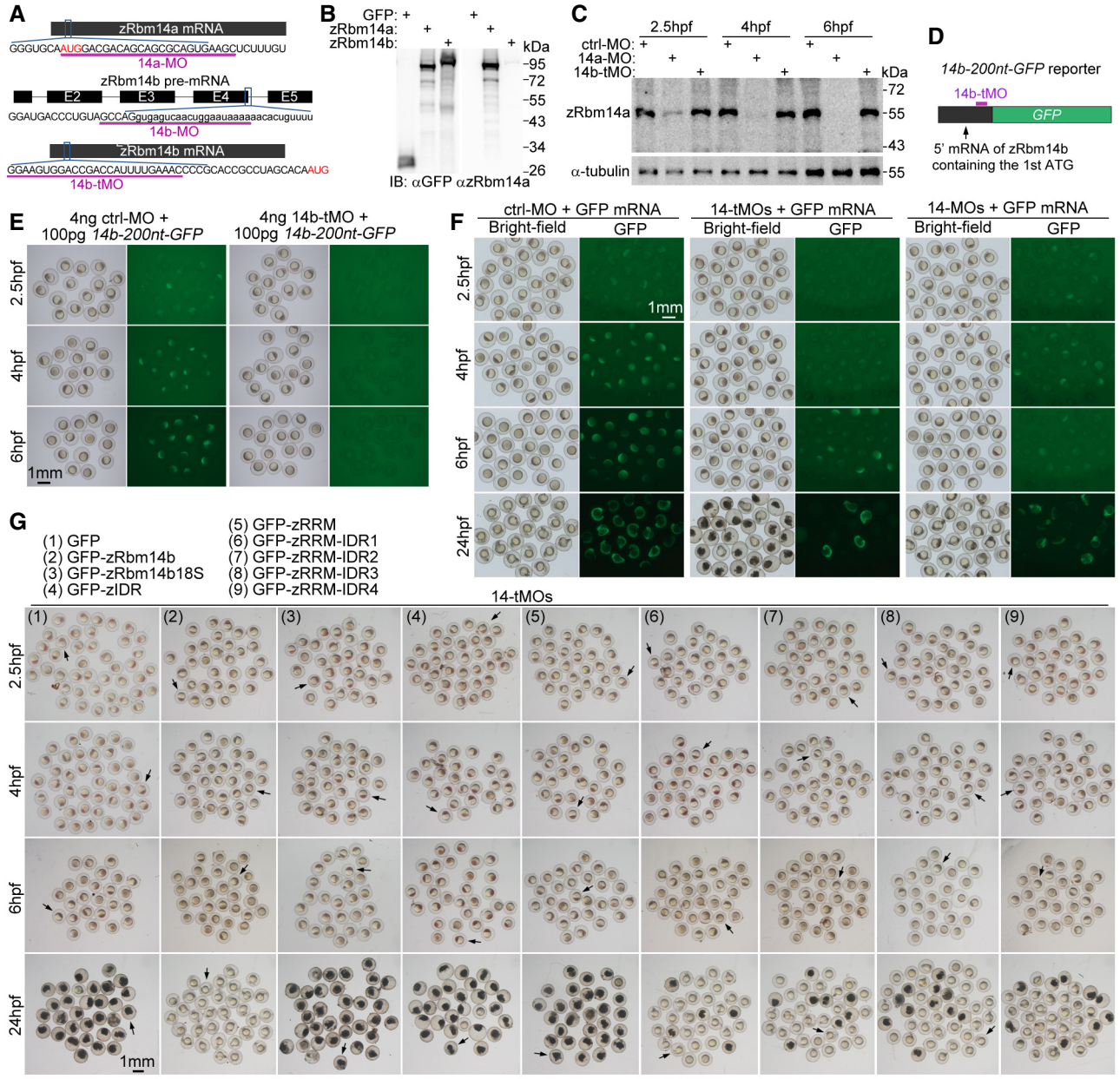

Figure EV2.

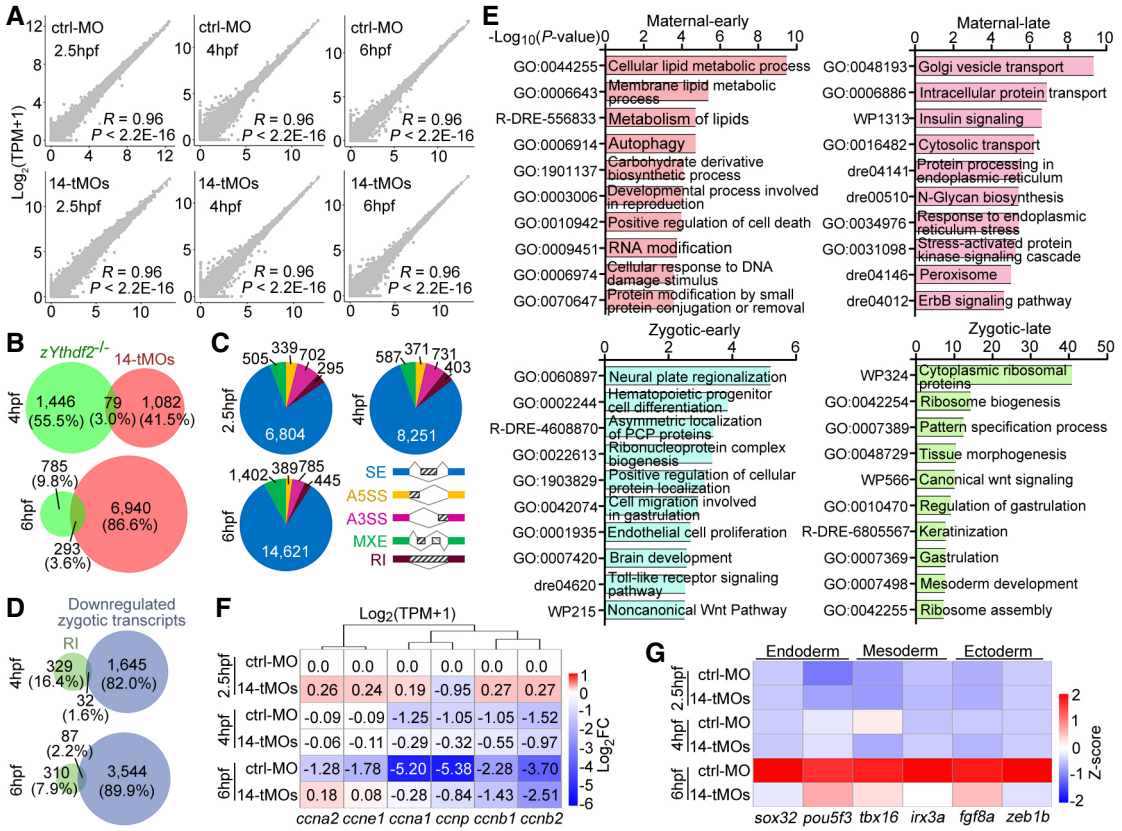

Figure EV3. Transcriptome analysis of zebrafish embryos (related to Fig 6).

A Scatter plots showing correlations of independent replicates of RNA-seq results. The Pearson correlation coefficient (R) and *P* values are shown.

B zRbm14 and zYthdf2 were largely responsible for the decay of different mRNAs. Only a small portion of transcripts accumulated in maternal zRbm14 morphants by more than 2-fold overlapped with those accumulated in maternal zYthdf2$^{-/-}$ embryos (Zhao *et al*, 2017). Note that the zRbm14 depletion interfered with the levels of much more transcripts than the zYthdf2 deficiency at 6 hpf.

C Differential alternative splicing events in the zRbm14 morphants. SE, skipped exon; A3SS, alternative 3′ splicing site; A5SS, alternative 5′ splicing site; MXE, mutually exclusive exon; RI, retained intron.

D Venn diagrams between the genes with differential RI and downregulated zygotic transcripts (Fig 6E) in maternal zRbm14 morphants. As the major ZGA occurs from 3 hpf (Fig 1A; Jukam *et al*, 2017), only transcripts of 4- and 6-hpf embryos were analyzed.

E Top 10 enriched terms of differentially expressed genes (DEGs, fold change > 2) between control and maternal zRbm14 morphants at 6 hpf.

F Relative transcript levels of cyclin genes. FCs were calculated from RNA-seq results, relative to the levels in 2.5-hpf ctrl-MO embryos, of two independent sets of samples. Only transcripts with TPM > 500 and classified as "maternal transcripts" (Fig 6D) were analyzed. Note the increasingly reduced clearance of the transcripts following time in maternal zRbm14 morphants. ccna1 and ccna2, zebrafish cyclin A genes; ccnb1 and ccnb2, cyclin B genes; ccne1, cyclin E gene; and ccnp, cyclin P gene.

G Expression profile of zygotic transcripts critical for the differentiation of three germ layers. Sox32 (also named casanova), pou5f3 (homolog of mammalian Oct4), tbx16 (spadetail), irx3a (encoding Iro3), fgf8a (encoding Fgf8a), and zeb1b (encoding Kheper) were selected from our pools of zygotic transcripts (Fig 6D) according to literature (Kudoh *et al*, 2004; Schier & Talbot, 2005; Perez-Camps *et al*, 2016).

Data information: *P* values of the sequencing data in (A) were calculated by using two-sided Wilcoxon and Mann–Whitney tests. *P* values in (E) were calculated by using Metascape. A *P* value of < 0.05 is considered statistically significant.
Source data are available online for this figure.

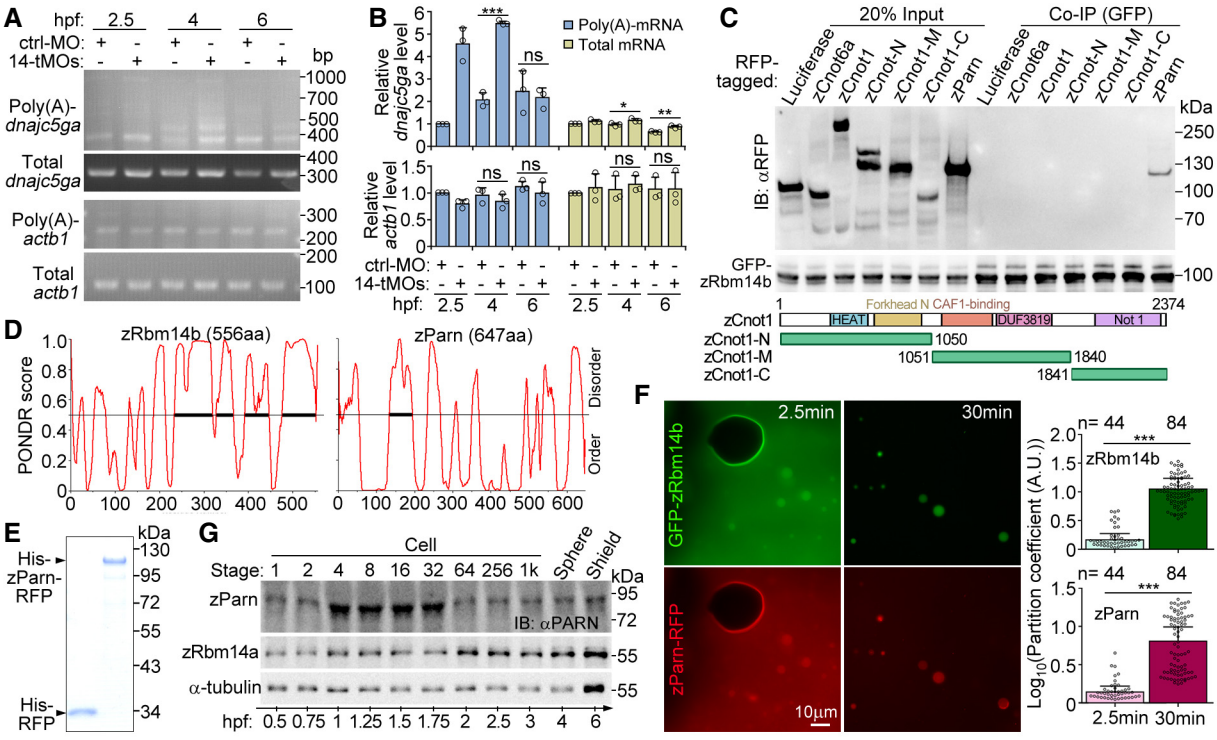

Figure EV4. Relationships between zRbm14 and zParn (related to Fig 7).

A, B Depletion of zRbm14 resulted in an accumulation of poly(A)-containing maternal transcripts of dnajc5ga. Total RNAs purified from the indicated zebrafish embryos were subjected to poly(A) length assays as illustrated in Fig 7A. Transcripts of actb1 (β-actin mRNA), which was not a target of zRbm14 based on Fig 6D and E, served as a negative control. One set of representative PCR results (A) and quantification results from three independent experiments (B) are presented. The major band of poly(A)-actb1 was quantified, as in Fig 7B. As poly(A)-dnajc5ga emerged as multiple bands, their total intensity was measured.

C zParn, but not components of the CCR4-NOT complex, associated with zRbm14b. GFP-zRbm14b was co-expressed with the indicated RFP-fusion proteins in HEK293T cells. Co-immunoprecipitations (co-IP) were performed with anti-GFP beads. Luciferase served as a negative control. zCnot6a, zebrafish CCR4a orthologue; zCnot1, zebrafish Not1 orthologue. Diagrams of zCnot1 mutants are provided.

D Secondary structure prediction for zRbm14b and zParn using Predictor of Natural Disordered Regions (PONDR). Bold line indicates predicted IDR.

E Purified RFP and zParn-RFP from *E. coli*. The proteins were subjected to SDS–PAGE, followed by Coomassie blue staining.

F Efficient co-phase separation of 10-μM zParn and 10-μM zRbm14b. Purified zParn-RFP was mixed with GFP-zRbm14b and imaged under a wide-field microscope at 2.5 and 30 min, respectively. Partition coefficients were respectively calculated for 44 or 84 droplets from three independent experiments and pooled together in the histograms.

G Expression profile of zParn during early embryogenesis. Lysates from 5 embryos were loaded in each lane. Immunoblotting was performed with an anti-human PARN antibody. α-tubulin and zRbm14a served as internal controls.

Data information: Quantification results are presented as mean ± SD, with sample dots. Unpaired two-sided Student's *t*-test: ns, no significance; $*P < 0.05$; $**P < 0.01$; $***P < 0.001$. Note that the *t*-test cannot be performed for the 2.5-hpf samples in (B) because the relative mRNA levels of the control samples were set as 1 and thus have no error bars.
Source data are available online for this figure.

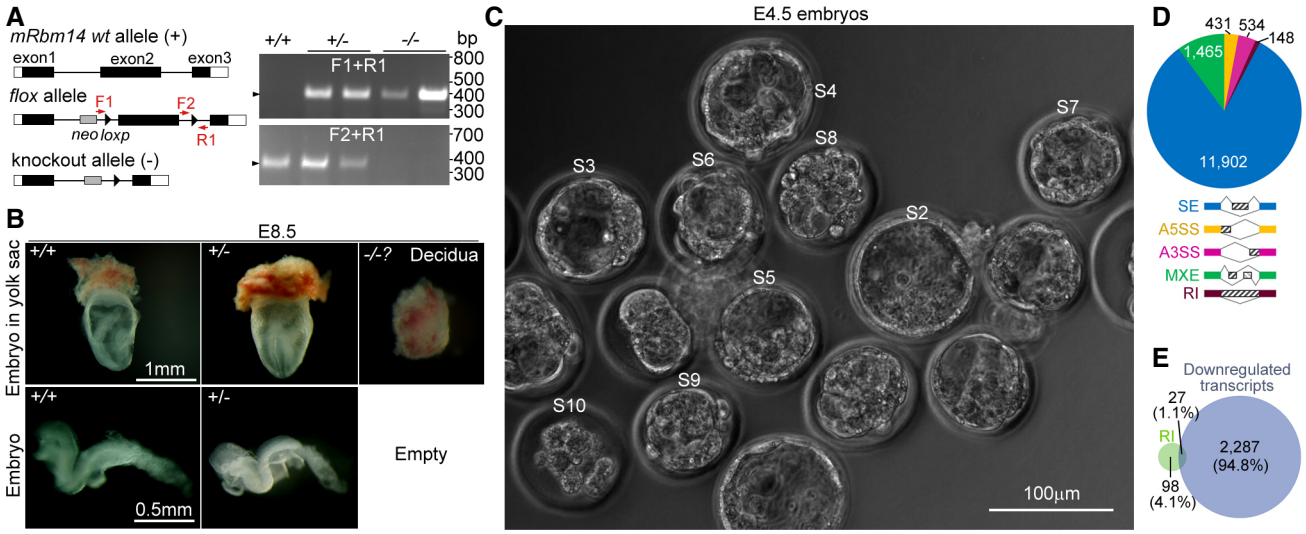

Figure EV5. Generation of *Rbm14*-deficient mice (related to Fig 8).

A Gene knock-out strategy and representative genotyping PCR results. The exon 2 of Rbm14 was knocked out by crossing Rbm14flox/flox mice with EIIa-Cre mice. Positions of two forward primers (F1 and F2) and the reverse primer (R1) for genotyping are indicated. Neo, neomycin resistance gene. The PCRs were performed using genomic DNAs from E8.5 embryos or remnants of resorbing Rbm14$^{-/-}$ embryos.

B Morphologies of mouse E8.5 embryos. No Rbm14$^{-/-}$ embryos were identified except for empty deciduae.

C E4.5 embryos used for RNA deep sequencing. Zygotic embryos were collected from the oviduct of superovulated Rbm14$^{+/-}$ female mice after mating with Rbm14$^{+/-}$ male mice and cultured to E4.5. Nine viable embryos (designated S2–S10) were picked as specimens for RNA extraction and deep sequencing.

D Differential alternative splicing events in Rbm14$^{-/-}$ embryos. SE, skipped exon; A3SS, alternative 3′ splicing site; A5SS, alternative 5′ splicing site; MXE, mutually exclusive exon; RI, retained intron.

E Venn diagrams between the genes showing differential RI and genes downregulated in the Rbm14$^{-/-}$ embryos (Fig 8F).

Source data are available online for this figure.